Soil Dynamics and Earthquake Engineering 113 (2018) 473–487

Contents lists available at ScienceDirect

Soil Dynamics and Earthquake Engineering

journal homepage: www.elsevier.com/locate/soildyn

Combination of dispersion curves from MASW measurements

Elin Asta Olafsdottir[a,*], Bjarni Bessason[a], Sigurdur Erlingsson[a,b]

[a] Faculty of Civil and Environmental Engineering, University of Iceland, Hjardarhagi 2-6, IS-107 Reykjavik, Iceland
[b] Pavement Technology, Swedish National Road and Transport Research Institute, SE-581 95 Linköping, Sweden

ARTICLE INFO

Keywords:
Multichannel analysis of surface waves
MASW
Dispersion curves
Measurement profile configuration
Combination
Stacking
Uncertainty analysis
Confidence intervals
Bootstrap

ABSTRACT

Multichannel analysis of surface waves (MASW) is a seismic exploration method for determination of near-surface shear wave velocity profiles based on analysis of horizontally travelling Rayleigh waves. This paper aims to propose a methodology and recommendations for combining dispersion data from several multichannel records. The dispersion curves are added up within logarithmically spaced wavelength intervals and the uncertainty of the mean phase velocity estimates is evaluated by using classical statistics and the bootstrap. The results indicate that combining multiple dispersion curves, which have been gathered by receiver spreads of different lengths (but with the same midpoint), can increase the investigation depth of the survey, improve its resolution at shallow depth and overall improve the reliability of the results as compared to the use of a single record. Moreover, the uncertainty of the combined mean dispersion curve can be determined and further used to present the shear wave velocity profile with upper and lower boundaries.

1. Introduction

The shear wave velocity (V_S) of near-surface materials is an important parameter in various geotechnical and earthquake engineering projects. The small-strain shear modulus of individual soil layers (G_0) is directly proportional to the square of their characteristic shear wave velocity. Furthermore, the shear wave velocity is fundamental in assessing soil amplification and for seismic site classification [1–3].

Several in-situ methods exist for evaluation of near-surface shear wave velocity profiles [1,4]. These include methods that require access to a drilled borehole, such as down-hole and cross-hole seismic surveys, methods where the resistance of soil to penetration is measured like the standard penetration test (SPT) and the cone penetration test (CPT), and surface wave analysis methods, such as the multichannel analysis of surface waves (MASW) method. Surface wave analysis methods utilize the dispersive properties of surface waves, commonly Rayleigh waves, propagating through a heterogeneous medium [5,6]. The shear wave velocity profile is subsequently obtained by backcalculation of the dispersion data by assuming a layered soil model. Compared to other available methods, surface wave analysis methods are low cost, as well as being non-invasive and environmentally friendly since they neither require heavy machinery nor leave lasting marks on the surface of the test site. Moreover, surface wave methods are applicable at a wide variety of sites, ranging from very fine grained silty soil sites to coarse grained gravelly sites, and even soft rock, hence, including locations where for example penetration tests are difficult to apply. MASW is a relatively new surface wave analysis technique [7,8] that has attracted an increased attention in recent years [9]. The main advantages of the MASW method, as compared to a two-receiver analysis [10], include a more efficient data acquisition in the field and improved data processing procedures where data from multiple receivers is analysed simultaneously [8]. Furthermore, the MASW method makes it possible to identify higher mode dispersion curves based on the recorded surface wave data [11].

Determination of experimental Rayleigh wave dispersion curves is a critical stage in the application of MASW. An inaccurate or erroneous experimental dispersion curve can cause severe errors in the back-calculated shear wave velocity profile [8,12,13]. At locations where the fundamental mode of the Rayleigh wave prevails, the retrieved fundamental mode wavelength range constrains the investigation depth range of the survey [14]. In short, the longer the maximum retrieved wavelength, the greater the prospective maximum investigated depth, and the shorter the minimum recorded wavelength, the better the resolution of the survey at shallow depth. The configuration of the measurement profile, including the length of the receiver spread (L) and the distance from the impact load point to the first receiver (x_1), is known to affect the acquired dispersion data [15–23]. The observed effects suggest that a wider range of dispersion curve wavelengths can be obtained by combination of data acquired using measurement profiles with different L and/or x_1 [16,17,24,25]. Furthermore, the acquired surface wave records are affected by correlated and uncorrelated noise sources. The manual aspect of the analysis, particularly the visual identification of dispersion curves based on images of

* Corresponding author.
E-mail addresses: eao4@hi.is (E.A. Olafsdottir), bb@hi.is (B. Bessason), sigger@hi.is (S. Erlingsson).

https://doi.org/10.1016/j.soildyn.2018.05.025
Received 5 May 2017; Received in revised form 25 February 2018; Accepted 23 May 2018
Available online 03 July 2018

processed data, also adds to the uncertainty associated with the dispersion curve estimates. Hence, when repeated measurements are carried out, some variability among the resulting dispersion curve estimates will be observed. Multiple records thus result in multiple curves, which combined may improve the estimation of the actual dispersion curve. As the individual dispersion curves may cover different wavelength ranges, the combined curve can include a wider range of wavelengths than any single experimental curve, and, hence, lead to an increased investigation depth range. Combination of dispersion data from several multichannel records can also be achieved by adding (stacking) multiple dispersion images before extracting a single dispersion curve. Stacking of multiple dispersion images can reduce noise and help identification of the fundamental mode dispersion curve [24,26–28]. By averaging the dispersion data post dispersion curve extraction, the uncertainty of the mean dispersion curve estimate can be evaluated, for instance, in terms of parametric or non-parametric confidence intervals for the mean dispersion curve. The uncertainty analysis can provide the analyst a more rational evaluation of the quality of the dispersion data and the combined dispersion curve. The uncertainty of the combined mean dispersion curve can further be utilized to present the shear wave velocity profile with upper and lower boundaries.

Few authors have obtained composite experimental dispersion curves with phase velocity uncertainties as a part of an active-source MASW survey. The combined curves have been constructed based on dispersion curves obtained by repeated shots [29,30], dispersion data gathered using different shot positions [21,31,32] or measurement profiles of different lengths [25]. Furthermore, in a few studies where the experimental dispersion curve has been identified from a stacked dispersion image, the experimental uncertainty has been assessed using the dispersion curves extracted from the single shot images [27,28]. However, in all above-mentioned studies, the main objective has not been computation of composite experimental dispersion curves, hence, the dispersion curve combination and uncertainty evaluation procedure is not well described and no general recommendations are given.

This paper aims to propose a methodology for combining dispersion curves from several multichannel records for the purpose of producing a reliable combined mean dispersion curve over a wide range of wavelengths. In this work, only the fundamental mode of Rayleigh wave propagation is considered. However, the methodology can be extended to higher modes as well. A number of records acquired by different measurement profile configurations at a silty sand test site are used to demonstrate the methodology. Recommendations for optimal measurement profile parameter/dispersion curve combinations in the context of ranges of wavelengths and phase velocities are presented. The uncertainty of the combined mean dispersion curve estimates was quantified, using both classical statistics and bootstrapping. The inverted shear wave velocity profiles are presented to further assess the effects of the different dispersion curve combinations. Similar results have been observed at other sandy test sites where the proposed methodology has been applied.

2. Multichannel analysis of surface waves

An application of MASW includes three steps; field measurements, dispersion analysis and inversion analysis [8]. An overview of the MASW method, as it is applied in this paper, is provided in Fig. 1. Surface waves are generated by an active seismic source and the wave propagation is recorded by multiple geophones that are evenly spaced along the survey line (Fig. 1a–c). Each multichannel surface wave record is transformed into a dispersion image and the corresponding (elementary) fundamental mode dispersion curve is identified (Fig. 1d–f). The elementary dispersion curves are subsequently combined into a single experimental curve and the uncertainty associated with the combined mean curve evaluated (Fig. 1g). Finally, the shear wave velocity profile is obtained by inversion of the combined mean dispersion curve by assuming a plane-layered elastic earth model (Fig. 1h–k). Under a mild lateral shear wave velocity variation, the backcalculated shear wave velocity profile can reasonably be assigned to the centre of the receiver spread [33].

In general, the resolution of surface wave analysis techniques, such as MASW, diminishes with increasing depth [34]. That is, while the analysis can resolve relatively thin layers and modest shear wave velocity variations close to the surface, only major variations in shear wave velocity/layering can be detected at greater depths. Furthermore, the fundamental mode Rayleigh wave dispersion curve is poorly sensitive to variations in material properties at depths greater than one third to half the maximum resolved wavelength (λ_{max}) [14,34,35]. Hence, a commonly used rule of thumb for interpretation of fundamental mode dispersion curves is to limit the maximum depth of the shear wave velocity profile (z_{max}) by the longest retrieved wavelength (e.g. [8,14,34,36]) as

$$z_{max} \leq \gamma \lambda_{max}, \quad \frac{1}{3} \leq \gamma \leq \frac{1}{2} \tag{1}$$

where γ is the ratio of the maximum depth of the shear wave velocity profile to the longest wavelength. Similarly, limiting the thickness of the top-most layer (h_1) by the shortest retrieved Rayleigh wave wavelength (λ_{min}) has been recommended (e.g. [8,14,36]), i.e.

$$h_1 \geq \zeta \lambda_{min}, \quad \frac{1}{3} \leq \zeta \leq \frac{1}{2} \tag{2}$$

where ζ is the ratio of the minimum thickness of the top-most layer to the shortest wavelength, as the fundamental mode dispersion data does not provide sufficient information to constrain the solution at shallower depths. When MASW surveys are carried out, the focus is commonly on achieving a particular investigation depth, and, therefore, on obtaining a certain maximum Rayleigh wave wavelength. However, as the shallowest soil layers have an influence on the entire experimental dispersion curve, information about the short wavelength wave components is also of importance [34]. Thus, even in cases where a detailed analysis of the shallowest soil layers is not a main objective, an experimental dispersion curve covering a wide range of wavelengths can be of value in order to constrain the inversion and increase the accuracy of the inverted shear wave velocity profile.

Ideally, the dispersion analysis should provide identification and extraction of the (elementary) dispersion curve for each mode. However, in-situ surface wave registrations are incomplete to some extent, imposing various challenges when dispersion curves are identified based on a dispersion image. Uncertainty associated with the experimental dispersion data can arise from an improper application of the middle-of-receiver spread assumption, measurement and sampling errors (e.g. due to limitations of the measurement equipment or an imprecise measurement profile set-up), and coherent or uncorrelated noise in the recorded signal [30,34,37]. Quantification of how the error associated with the recorded surface waves is propagated through the different data processing steps has however been reported as problematic [30]. Direct estimates of the statistical distributions of the extracted phase velocity values (i.e. at each wavelength/frequency) can nevertheless provide a measure of the error associated with the Rayleigh wave dispersion data. The processing of the recorded data and the dispersion curve identification/extraction can further introduce uncertainty in the experimental dispersion curves [30,34,37]. The fundamental mode of Rayleigh wave propagation typically prevails at sites where the shear wave velocity increases gradually with increasing depth [12,34,38,39]. At sites characterized by a more irregularly varying stiffness profile, higher modes can play a significant role in certain frequency ranges, thus making the identification of the fundamental mode dispersion curve difficult. In such cases, misidentification of mode numbers or superposition of dispersion data from two (or more) modes can occur, resulting in an apparent dispersion curve that does not correspond to any of the real modes [12,13,34]. A further source of uncertainty is potential inter-analyst variability associated

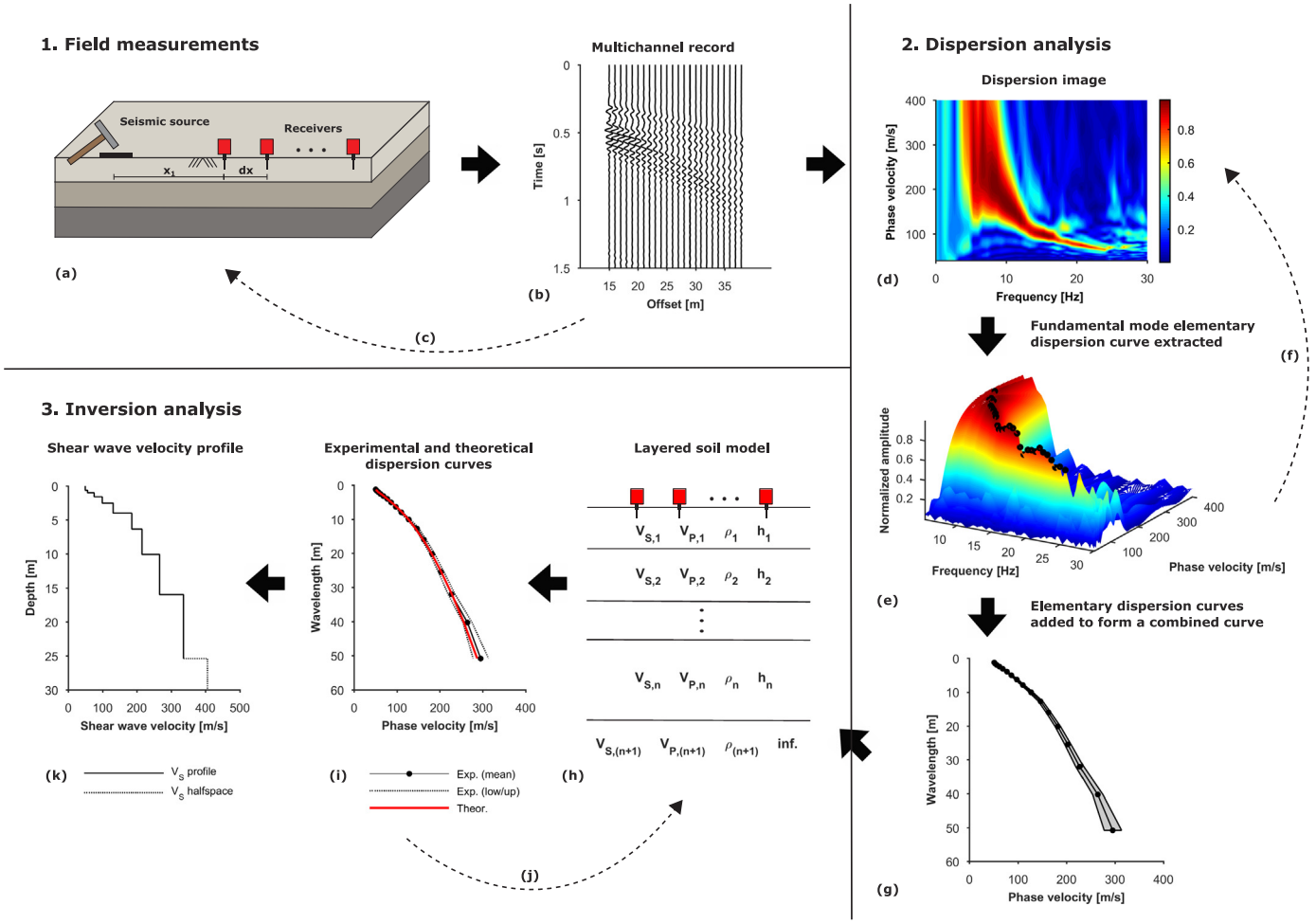

Fig. 1. Application of the MASW method. (a) Geophones are lined up on the surface of the test site with equal receiver spacing dx. A wave is generated using an impulsive source that is applied at a distance x_1 from one end of the receiver spread. (b) The wave propagation is recorded. (c) Steps (a) and (b) are repeated several times using different values of dx and/or x_1, while keeping the midpoint of the receiver spread fixed. (d) A dispersion image is obtained based on each multichannel surface wave record. (e) The high-amplitude bands display the dispersion characteristics and are used to identify the elementary fundamental mode Rayleigh wave dispersion curve. (f) Steps (d) and (e) are carried out for each acquired surface wave record. (g) The extracted elementary dispersion curves are added up to obtain a combined mean experimental curve along with upper/lower boundary curves. (h) An initial estimate of a layered soil model for the test site is obtained. The parameters required to describe the properties of each layer are shear wave velocity (V_S), compressional wave velocity (V_P), mass density (ρ) and layer thickness (h). The last layer is assumed to be a half-space. (i) A theoretical dispersion curve is computed based on the assumed soil model and compared to the combined mean experimental dispersion curve. (j) The layered soil model is updated and the theoretical dispersion curve is recomputed until the misfit between the theoretical and experimental curves has reached an acceptably small value. (k) The shear wave velocity profile and the layer structure that result in an acceptable fit, and can realistically represent the characteristics of the test site, are taken as the results of the survey.

with the manual or semi-manual dispersion curve picking. The human bias may, however, be limited by averaging dispersion curve picks obtained by several analysts [37]. In general, the low frequency (longer wavelength) part of the dispersion curve is characterized by higher uncertainty than the higher frequency (shorter wavelength) region [30].

It is further commonly recognised that the configuration of the measurement profile can affect the quality of the dispersion image that is obtained [15–23] and consequently the uncertainty associated with the dispersion curve identification and extraction. In general, given that the lateral changes in shear wave velocity are small, an increased length of the receiver spread provides improved spectral resolution. The high-amplitude peaks observed at each frequency appear sharper and better separation between different modes of surface wave propagation is observed [16,17], thus facilitating the dispersion curve picking. A longer receiver spread is also preferred in order to acquire the lower frequency (longer wavelength) Rayleigh wave components that provide the deepest part of the shear wave velocity profile. However, an increased receiver spread length risks attenuation of higher frequency (shorter wavelength) fundamental mode components (which reduces the minimum resolvable investigation depth) and spatial aliasing if a fixed number of geophones is used [34,40]. Furthermore, an increased length of the receiver spread risks significant lateral variations in material properties along the geophone array [16]. The analysis is based on the assumption that the wave front of the Rayleigh wave is plane. In general, the length of the source offset has to be sufficient to assure plane wave propagation of surface wave components [16,20,41]. The minimum source offset required to avoid near-field effects depends on the longest wavelength that is analysed. A very short source offset can result in an irregular and unreliable high-amplitude trend in the dispersion image at lower frequencies, usually displaying lower phase velocities than images free of this effect. An overly long source offset, however, risks excessive attenuation of fundamental mode components at higher frequencies.

3. Dispersion analysis

The objective of the dispersion analysis is to identify experimental

dispersion curves based on the acquired multichannel surface wave records. Transform-based methods, in which the multichannel time series are transformed from the space-time domain into a different domain, are most commonly used for active-source surveys [6], i.e. the frequency–wave number (f–k) transform [42], the slowness–frequency (p–ω) transform [43] and the phase shift method [44]. A comparison of the effectiveness of the three methods has revealed that the phase shift method is a robust and computationally effective method that provides accurate fundamental mode phase velocities, even when data from only a limited number of geophones are available [45]. Hence, in this work, the acquired surface wave records were analysed by the phase shift method. Identification and extraction of elementary dispersion curves was carried out by using the open source Matlab software MASWaves [46] (see also masw.hi.is). The original dispersion analysis tool of MASWaves was modified in order to include the proposed methodology for combining dispersion curves from several records.

An application of the phase shift method can be divided into three main steps; (i) Fourier transformation and amplitude normalization, (ii) dispersion imaging, and (iii) identification/extraction of dispersion curves [44,47]. The multichannel surface wave record is denoted by $u(x_j, t)$ where x_j is the distance from the impact load point to the j-th receiver and is time. The number of geophones is denoted by N. First, each trace of the multichannel record is transformed into the frequency domain by a Fourier transform. The j-th trace of the transformed record $\tilde{u}(x_j,\omega)$ can be expressed in terms of its amplitude $A_j(\omega)$ and phase $\Phi_j(\omega)$ as

$$\tilde{u}(x_j, \omega) = A_j(\omega)\exp(-i\Phi_j(\omega)) = A_j(\omega)\exp\left(-i\frac{\omega x_j}{c(\omega)}\right) \tag{3}$$

where $c(\omega)$ is the characteristic phase velocity of the frequency component ω, $\Phi_j(\omega)= \frac{\omega x_j}{c(\omega)}$ and $i^2 = -1$. The amplitude of the transformed record does not include any information on phase velocity. Hence, $\tilde{u}(x_j,\omega)$ is normalized in order to remove the effects of geometrical spreading and attenuation on the acquired data. The analysis is thus concentrated on the phase velocity effect only.

$$\tilde{u}_{norm}(x_j, \omega) = \frac{\tilde{u}(x_j, \omega)}{|\tilde{u}(x_j, \omega)|} = \exp\left(-i\frac{\omega x_j}{c(\omega)}\right) \tag{4}$$

For a given testing phase velocity (c_T) and a given frequency (ω), the amount of phase shifts required to counterbalance the time delay corresponding to specific offsets (x_j) is determined. The phase shifts are applied to distinct traces of $\tilde{u}_{norm}(x_j,\omega)$ that are thereafter added to obtain the slant-stacked amplitude $S(\omega,c_T)$ corresponding to the ordered couple (ω,c_T)

$$S(\omega, c_T) = \frac{1}{N}\sum_{j=1}^{N}\exp\left(-i\frac{\omega x_j}{c_T}\right)\tilde{u}_{norm}(x_j, \omega) \tag{5}$$

The summation operation described by Eq. (5) is repeated for all the different frequency components of the transformed record in a scanning manner using varying testing phase velocity values. When the testing phase velocity becomes equal to the true phase velocity $c(\omega)$ a maximum is observed in $S(\omega,c_T)$. The values of $S(\omega,c_T)$ are visualized as a two (or three) dimensional dispersion image (phase velocity spectrum). The spectral high-amplitude bands display the dispersion characteristics of all types of waves contained in the recorded data (Fig. 1d) and are used to identify and extract the elementary Rayleigh wave dispersion curve(s) (Fig. 1e).

For determination of a combined mean dispersion curve (Fig. 1 g), assume that m multichannel surface wave records have been obtained at the same location (i.e. by using measurement profiles with the same midpoint and possibly different receiver spread lengths and/or different source offsets). Each surface wave record is processed separately (e.g. by use of the phase shift method) resulting in m experimental elementary dispersion curves. Each elementary curve consists of n_j data points $(c_{j,l}, \lambda_{j,l})$ (where $l = 1,..., n_j$ and $j = 1, ...,m$).

The combined mean experimental dispersion curve, denoted by $(c_{e,q}, \lambda_{e,q})$ (where $q = 1, ...,Q$) is obtained by grouping the data points included in the m elementary dispersion curves together within $\log_a$ spaced (i.e. a^{-1}th octave) wavelength intervals $[\lambda^L_{e,q}, \lambda^U_{e,q})$. Q is the number of wavelength intervals, $\lambda_{e,q}$ is the reference point of the q-th interval and $\lambda^L_{e,q}$ and $\lambda^U_{e,q}$ are its upper and lower bounds, respectively. Hence, the wavelengths that characterize the q-th interval are obtained as

$$\begin{aligned}\lambda_{e,q} &= 2^{\frac{q-1}{a}}\\ \lambda^L_{e,q} &= \lambda_{e,q}\cdot 2^{-\frac{1}{2a}}\\ \lambda^U_{e,q} &= \lambda_{e,q}\cdot 2^{\frac{1}{2a}}\end{aligned} \tag{6}$$

Subsequently, all phase velocity values $c_{j,l}$ such that $\lambda_{j,l}\in[\lambda^L_{e,q}, \lambda^U_{e,q})$ are added up and their arithmetic mean (denoted by $c_{e,q}$) used as a point estimate of the phase velocity of Rayleigh wave components belonging to the given wavelength range.

4. MASW dispersion data

4.1. Field measurements

Multichannel surface wave records were acquired in 2015 at Arnarbæli in Ölfus, South Iceland. The soil at the Arnarbæli site consists of a relatively homogeneous glaciofluvial volcanic sand deposited on the western bank of the estuary of the Ölfus River [48,49]. The surface wave records were collected using a linear array of 24 vertical geophones with a natural frequency of 4.5 Hz. Three measurement profiles with the same midpoint but varying receiver spacing (dx) were tested, i.e. $dx = 0.5$ m, $dx = 1.0$ m and $dx = 2.0$ m. For each receiver spacing, four different source offsets (x_1) were used. For each combination of dx and x_1, six surface wave records (where each record consisted of 24 time series) were acquired, resulting in a total of 72 records. The impact load was in all cases created by a 6.3 kg sledgehammer. The high number of records gathered using multiple measurement profile configurations makes this dataset an appropriate choice for testing the proposed methodology. A summary of the main parameters related to the field measurements is provided in Table 1.

4.2. Dispersion curves

Each multichannel record was processed separately by using the

Table 1
Overview of site characteristics and MASW test configuration at the Arnarbæli test site.

Site characteristics			
Soil type			Holocene glaciofluvial sand
USCS classification			SW-SM
Location of groundwater table			At surface
Saturated mass density	ρ_{sat}	[kg/m^3]	1850
Field measurements			
No. geophones	N		24
No. profiles			3
Receiver spacing (source offsets)	dx (x_1)	[m]	0.5 (3.0/5.0/7.5/10.0) 1.0 (5.0/10.0/15.0/25.0) 2.0 (5.0/10.0/15.0/25.0)
No. measurements per combination of dx and x_1			6
Sampling rate	f_s	[Hz]	1000
Recording time	T	[s]	2.4

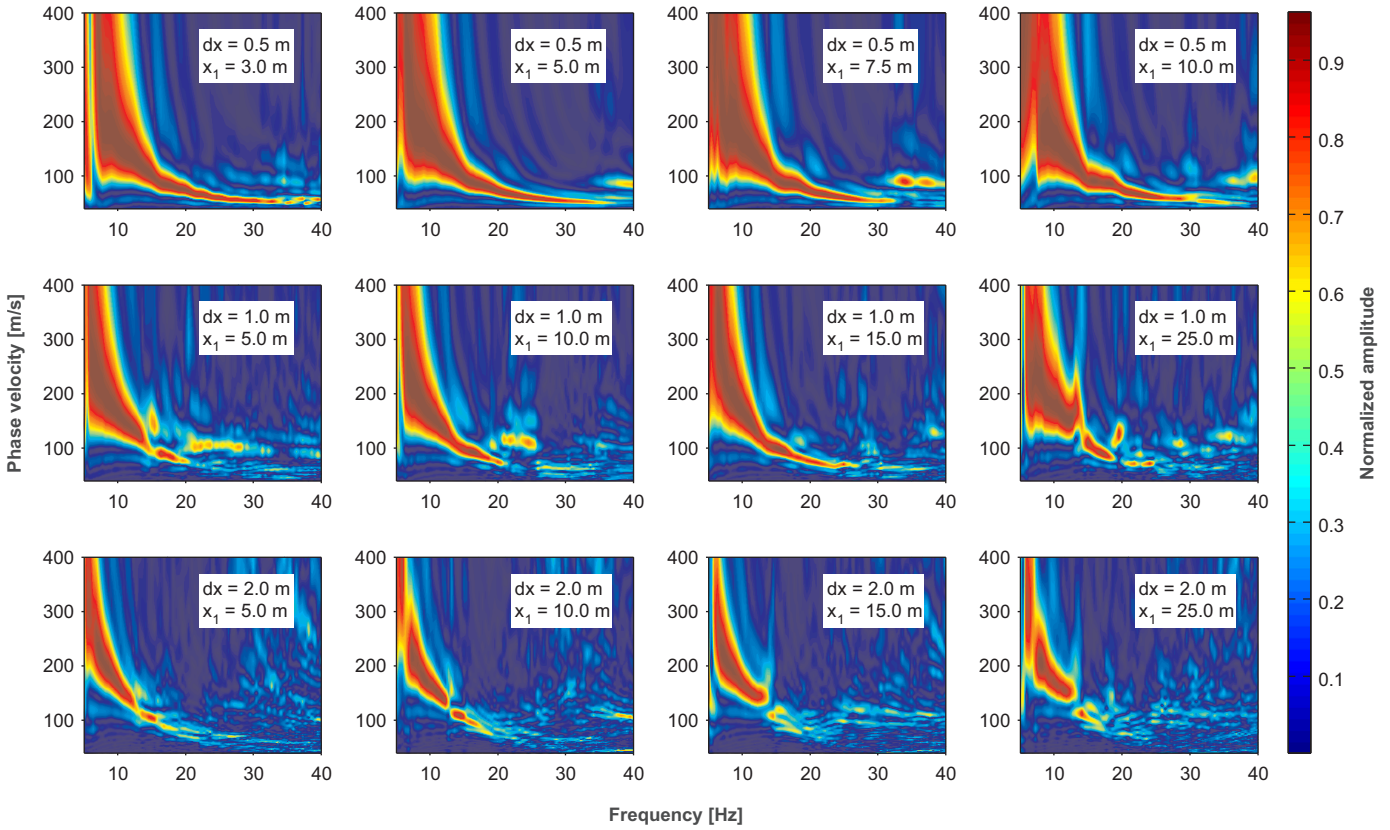

Fig. 2. Dispersion images of multichannel surface wave records acquired with receiver spreads of different lengths and with different source offsets.

phase shift method. The variability among the extracted elementary dispersion curves was subsequently evaluated in terms of the coefficient of variation (C_V) among the estimated phase velocity values at each frequency

$$C_V = \frac{s_c}{\bar{c}} \tag{7}$$

where $\bar{c}$ is the average of the estimated phase velocity values at frequency f and s_c is the corresponding standard deviation (SD).

Typical dispersion images of records acquired with each measurement profile configuration are shown in Fig. 2. The fundamental mode dispersion curves that were identified based on the data are presented in Fig. 3a. The dispersion curve estimates obtained by using diverse measurement profile configurations agreed well, being characterized by a C_V between 1% and 8% at each frequency (Fig. 3b). As expected, the lowest frequency components displayed more variability than components in the higher frequency range.

As shown in Fig. 2, the configuration of the measurement profile, i.e. the length of the receiver spread and the source offset, had a considerable effect on the dispersion images that were obtained, and subsequently on the retrievable dispersion curve frequency range in each case. Time series recorded by the shortest receiver spread provided in general the most information about the dispersion properties of the short wavelength (higher frequency) wave components that propagated through the top-most soil layers (Fig. 3a). However, with increasing receiver spread length, the observed spectral resolution increased (Fig. 2) which facilitated the identification of the fundamental mode at lower frequencies (Fig. 3a). Hence, time series recorded by the longer receiver spreads tended to provide the greatest investigation depth. The observations were in accordance with existing recommendations where

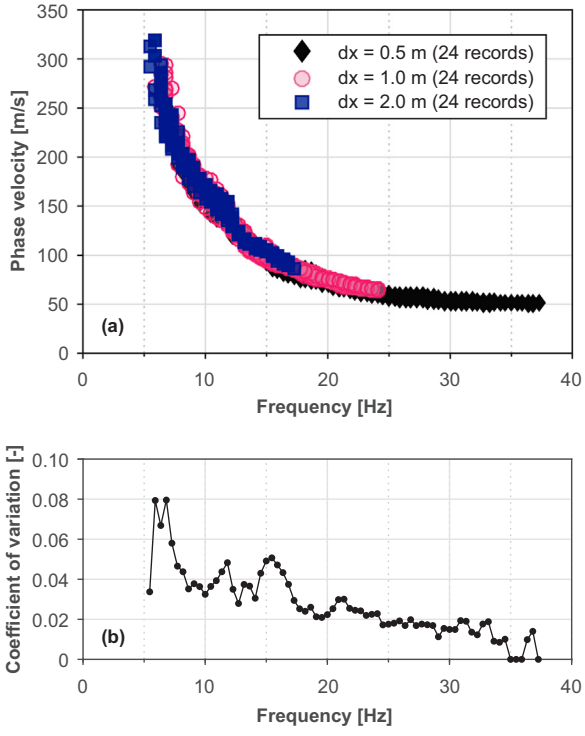

Fig. 3. (a) Fundamental mode dispersion curve estimates obtained by using receiver spreads of different lengths. (b) Variation of extracted Rayleigh wave phase velocity values at each frequency.

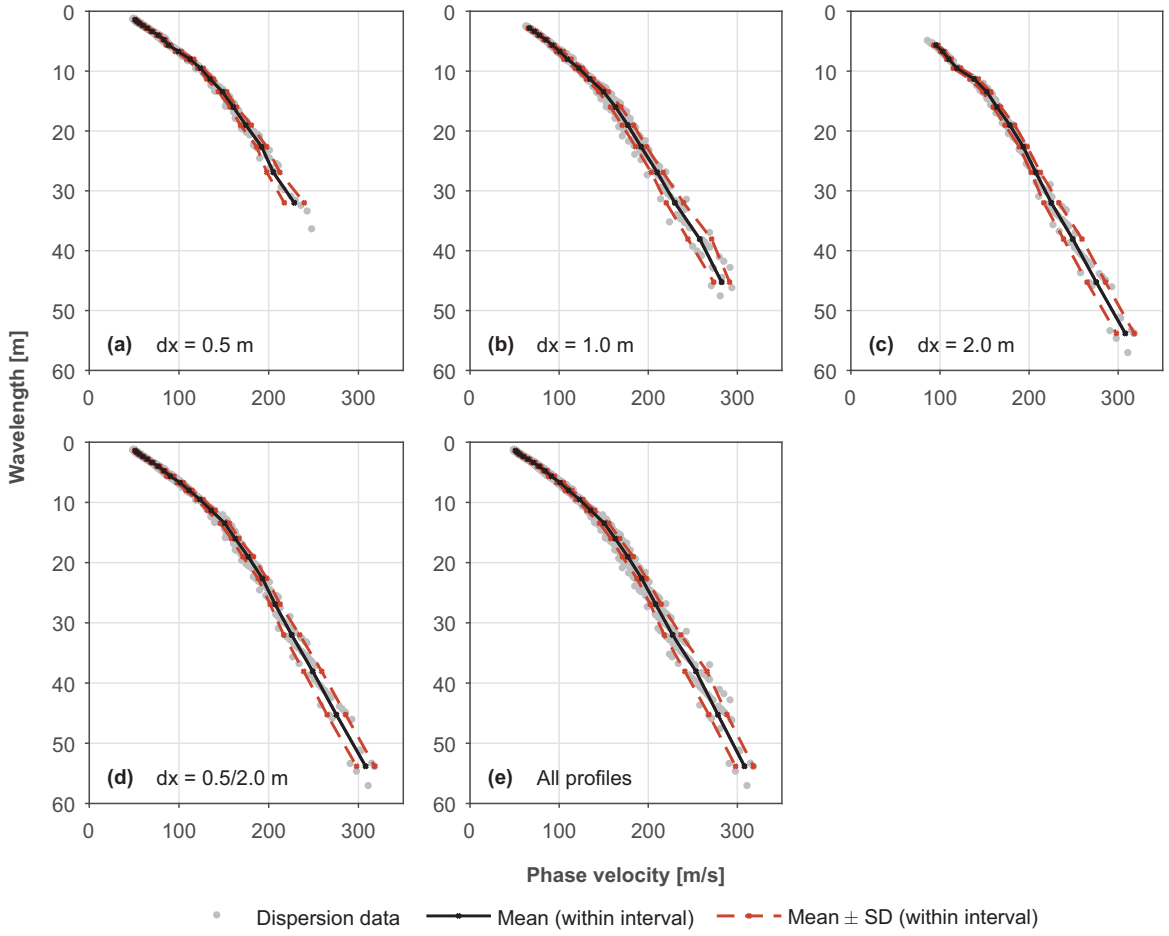

Fig. 4. Elementary dispersion curve data points and combined mean dispersion curves with upper and lower bound curves (mean ± one standard deviation) for the three profiles and the two profile combinations (with a = 4. 0 in Eq. (6)).

the obtainable investigation depth is suggested as directly related to the length of the receiver spread [20].

5. Combining dispersion curves

Fig. 4 illustrates the computation of composite dispersion curves for the three profiles (same midpoint) and the two profile combinations tested at the Arnarbæli site. The combined mean curves in Fig. 4a–c were obtained by grouping data points from each set of 24 elementary curves (i.e. 24 curves for the dx = 0.5 m profile, the dx = 1.0 m profile and the dx = 2.0 m profile, respectively) together within $\log_4$ spaced wavelength intervals, i.e. with a = 4.0 in Eq. (6). The optimal width and number of wavelength intervals was determined after initial inspection of the data (see further in Section 5.1). The mean phase velocity within each interval was used as an estimate of the phase velocity of the Rayleigh wave components belonging to the given wavelength range. The upper and lower bound curves shown in Fig. 4 correspond to plus/minus one standard deviation from the combined mean curve; hence, the upper and lower bound curves provide a measure of the spread of the elementary dispersion curve data points within each wavelength interval. In general, the spread of the data points increased with increased wavelength. Furthermore, the number of points associated with each wavelength interval decreased with increasing wavelength.

As indicated by the dispersion data shown in Fig. 3a, there was a considerable difference in the dispersion curve wavelength range that could be achieved by using each of the three profiles. The shortest (dx = 0.5 m) profile provided combined dispersion curve wavelengths in the range of 1.4–32.0 m (Fig. 4a), the intermediate length (dx = 1.0 m) profile provided wavelengths in the range of 2.8–45.3 m (Fig. 4b), and the longest (dx = 2.0 m) profile provided wavelengths in the range of 5.7–53.8 m (Fig. 4c).

The dispersion curves obtained by combining (i) the 48 dispersion curves acquired by the dx = 0.5 m and dx = 2.0 m profiles and (ii) the 72 dispersion curves acquired by all three profiles within $\log_4$ spaced wavelength intervals are shown in Fig. 4d and Fig. 4e, respectively. In both cases, the minimum combined curve wavelength was 1.4 m and the maximum wavelength was 53.8 m.

5.1. Number and width of wavelength intervals for combined dispersion curves

The number and width of wavelength intervals used for computation of a combined dispersion curve is controlled by the parameter a in Eq. (6). The width of each interval is inversely related to the value of a. Simultaneously, the number of intervals within a given wavelength range increases with increasing value of a. This is illustrated in Fig. 5. The reference wavelength value for each interval ($\lambda_{e,q}$) is specially indicated by a dot. As the interval length is logarithmically distributed, the effect of the different a-values on the interval length becomes more apparent with increasing wavelength.

The optimum value of a varies with dataset and should be chosen after initial inspection of the available data. Fig. 6 shows the effects of using selected values of the parameter a, i.e. a = 2.0, a = 3.0, a = 5.0 and a = 7.0, for computation of a composite dispersion curve based on the dispersion data acquired by the dx = 0.5 m and dx = 2.0 m profiles at the Arnarbæli site. The elementary dispersion curve data points that

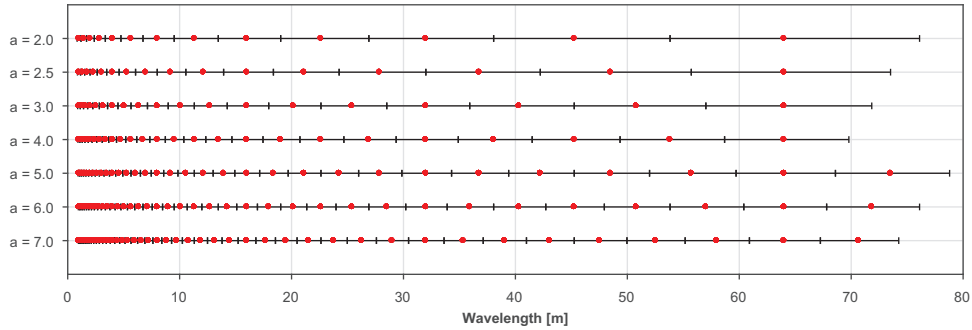

Fig. 5. Effects of the parameter a in Eq. (6) on the length and range of the wavelength intervals used for computation of a combined dispersion curve (here shown for assumed elementary dispersion curve wavelengths in the range of 1 m to approximately 70–80 m). The reference point for each wavelength interval ($\lambda_{e,q}$) is indicated by a dot.

fall within each wavelength interval (indicated by the alternating grey and white bands) are shown in Fig. 6a–d. The resulting combined mean dispersion curves are shown in Fig. 6e–h. The upper and lower bound curves also shown correspond to plus/minus one standard deviation from the combined mean curve in each case. The combined mean, upper and lower bound dispersion curves that were obtained for the same dataset by using $a = 4.0$ are shown in Fig. 4d. A comparison of the combined mean dispersion curves obtained by using the a values illustrated in Fig. 5 is provided in Fig. 7.

The results presented in Figs. 6 and 7 indicate that the selection of a did not have a substantial effect on the combined mean dispersion curve at wavelengths shorter than approximately 40 m. However, for longer wavelengths, where the wavelength intervals were wider and fewer data points were available, the effects of the different values of a become more visible.

The ideal value of a depends on the number and distribution of the available elementary dispersion curve data points. Based on present experience with applying the methodology, the following factors are of main importance for selection of a: (i) the elementary dispersion curve

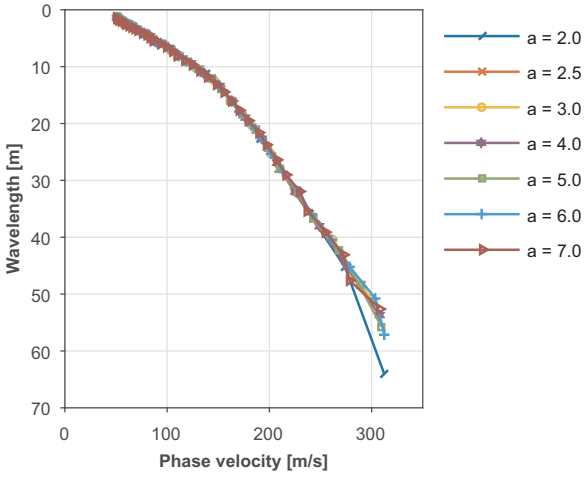

Fig. 7. Comparison of combined mean dispersion curves obtained by using different values of the parameter a in Eq. (6).

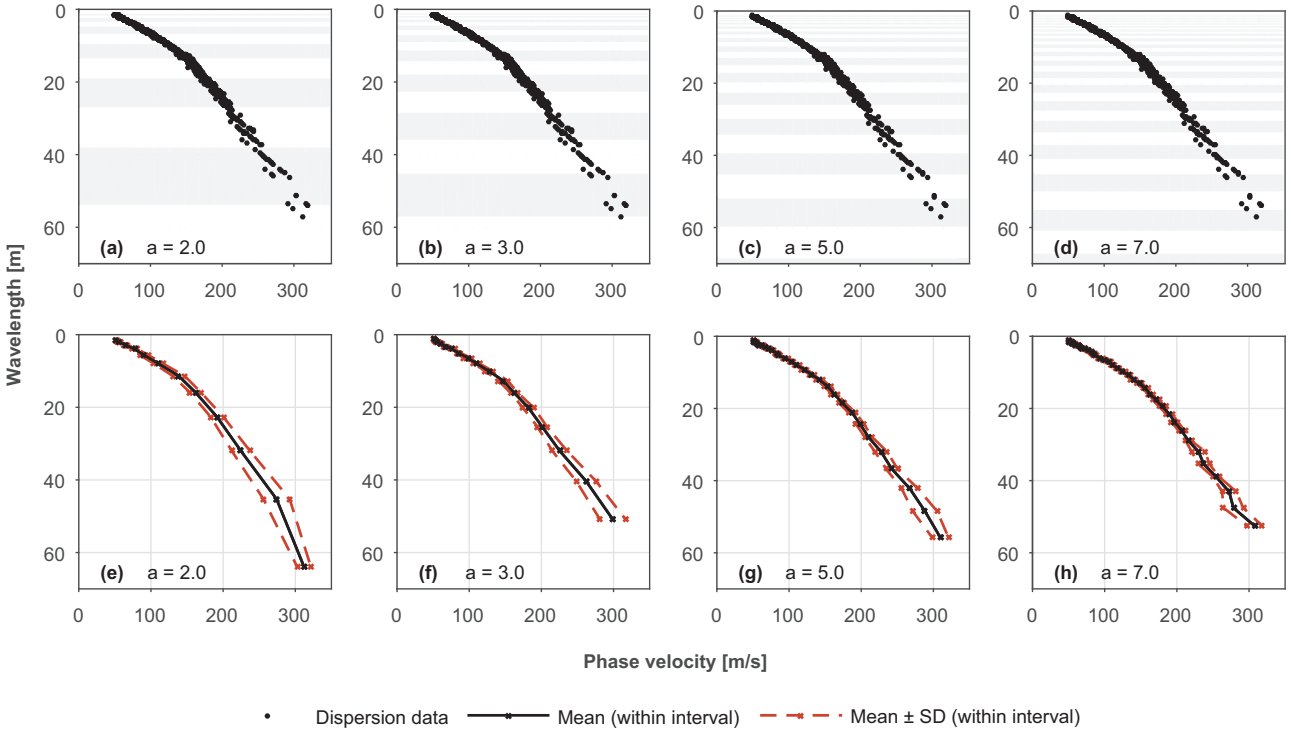

Fig. 6. Effects of using different values of the parameter a in Eq. (6) for determination of a combined mean dispersion curve. The combined curves are obtained based on the dispersion data acquired by the $dx = 0.5$ m and $dx = 2.0$ m profiles.

data points should be approximately evenly distributed within each wavelength interval, (ii) a sufficient number of data points should fall within each interval, and (iii) a higher value of a is in general preferable to a lower value.

An uneven distribution of the elementary dispersion curve data points or an insufficient number of data points falling within certain wavelength intervals can either result in an underestimated or overestimated combined curve phase velocity value ($c_{e,q}$) for the given wavelength range $[\lambda_{e,q}^{L}, \lambda_{e,q}^{U})$ (see e.g. the last wavelength interval, $\lambda \in [53.8, 76.1)$ m, in Fig. 6a, e). "Zigzagging" of the combined mean curve can be observed if either occurs for multiple adjacent wavelength intervals (see Fig. 6d, h). Moreover, an uneven distribution of the elementary dispersion curve data points can manifest itself by an increased standard deviation of the phase velocity values for the given interval (see e.g. the second last wavelength interval, $\lambda \in [45.3, 52.0)$ m, in Fig. 6c, g). In cases where the dispersion curve data points cluster together, there is also a risk that the standard deviation is not representative of the actual variability of the phase velocity values of the wave components that belong to the given wavelength range.

In general, the highest value of a that does not cause any of the previously described complications should be used. Increasing the number of wavelength intervals both provides more data points in the combined mean dispersion curve and, in general, decreases the uncertainty associated with its computation. Present experience with applying the methodology indicates that the optimum value of a for most test sites is in the range from $a = 2.5$ to $a = 5.0$. A default or initial value of $a = 3.0$ or $a = 4.0$ will in many cases be sufficient.

5.2. Number of elementary dispersion curves

The effects of using different number of elementary dispersion curves for computation of a combined mean curve for the Arnarbæli site are reported in Figs. 8–10. For each measurement profile/profile combination, the use of one, two, four and six multichannel surface wave records for each source offset was studied. Moreover, the effects of stacking two and four dispersion images, respectively, prior to identification of elementary dispersion curves, are shown and compared to the use of elementary curves identified based on single records. Hence, the use of a total of 30 elementary dispersion curve combinations was studied. An overview of the dispersion curve combinations and the number of elementary dispersion curves included in each combination is provided in Table 2.

Fig. 8 illustrates the grouping of the elementary dispersion curve data points into $\log_4$ spaced wavelength intervals (with $a = 4.0$ in Eq. (6)) for selected study cases, i.e. the $dx = 0.5$ m profile and the $dx = 0.5$ m/$dx = 2.0$ m combination. Also shown is the combined mean dispersion curve obtained for each case. The data acquired by the $dx = 1.0$ m profile, the $dx = 2.0$ m profile and the $dx = 0.5$ m/$dx = 1.0$ m/$dx = 2.0$ m combination, respectively, showed essentially the same characteristics as the data that is presented in Fig. 8.

The number of data points that fell within each wavelength interval for each of the 30 elementary dispersion curve combinations is reported in Fig. 9. By combining elementary dispersion curves obtained by profiles of different lengths (i.e. $dx = 0.5$ m/$dx = 2.0$ m or $dx = 0.5$ m/$dx = 1.0$ m/$dx = 2.0$ m) a more even distribution of the dispersion curve data points was obtained, as well as a substantially increased wavelength range, as previously described.

The combined mean dispersion curves that were obtained for each elementary curve combination are compared in Fig. 10. The agreement between the curves reported was in all cases good with a coefficient of variation (Eq. (7)) less than 2.5% for each reference wavelength. At wavelengths shorter than approximately 30 m, the combined mean curves were nearly identical. However, at longer wavelengths a minor difference between the curves was observed.

In general, the results indicate that in order to obtain the longest possible combined curve wavelength, it is preferable to use several (e.g. four or six) elementary dispersion curves for each profile length/source offset, rather than using a single record for each configuration. When a small number of records is used for computation of a combined curve (i.e. one or two records for each combination of dx and x_1) there is the risk of an inadequate number of elementary dispersion curve data points falling within each wavelength interval. In general, the fundamental mode dispersion curve trend of the longer wavelength (lower frequency) wave components is the most difficult to identify and to confidently extract from a dispersion image. Moreover, the mapping of the dispersion curve data points from the frequency-phase velocity domain into the phase velocity-wavelength domain spreads the lower

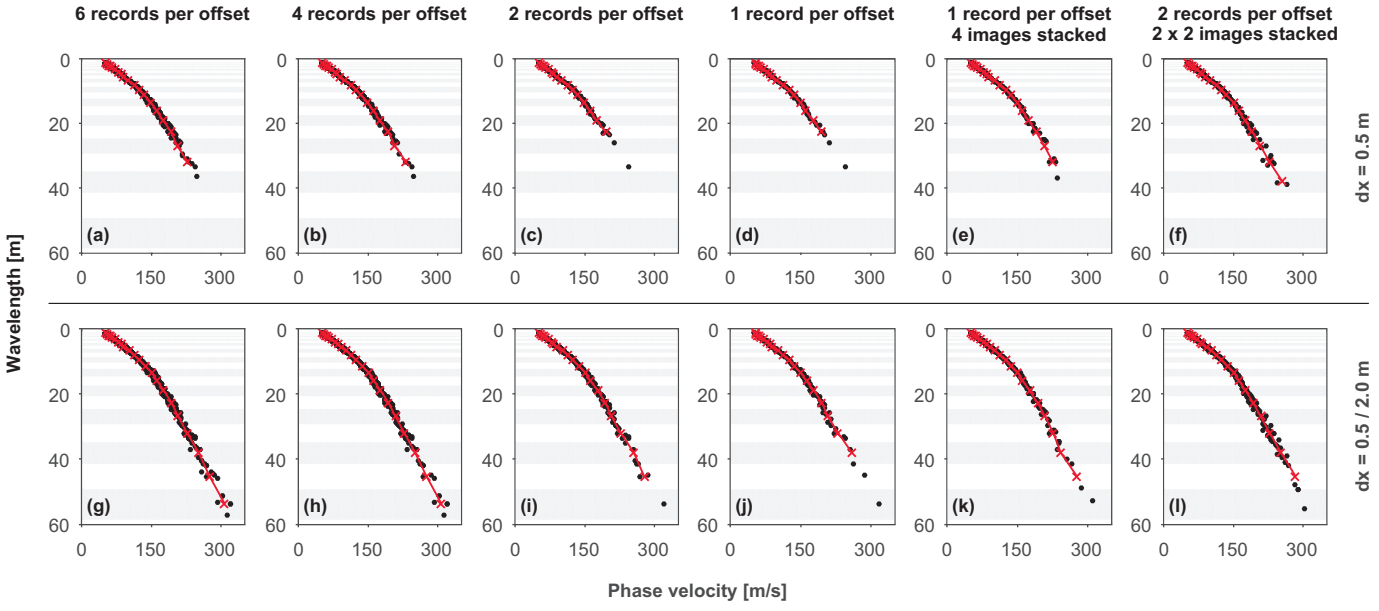

Fig. 8. Grouping of elementary dispersion curve data points into $\log_4$ spaced wavelength intervals (with $a = 4.0$ in Eq. (6)) for selected study cases from Table 2. The combined mean dispersion curve obtained for each case is shown with an unbroken line.

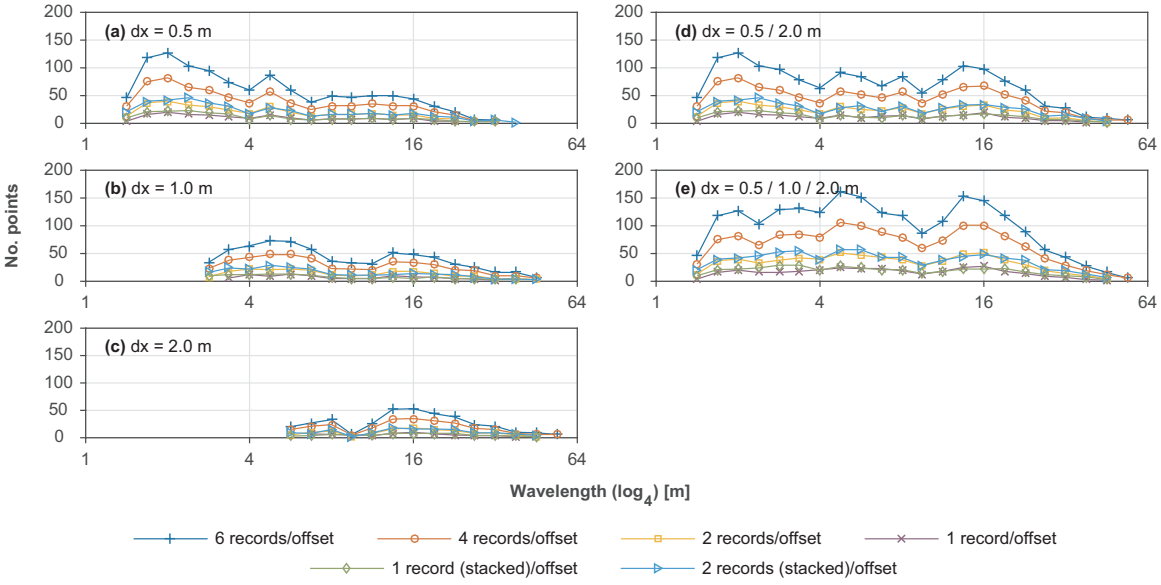

Fig. 9. Number of dispersion curve data points that fell into each $\log_4$ spaced wavelength interval (with $a = 4.0$ in Eq. (6)) for the study cases in Table 2.

frequency data points further apart than data points corresponding to higher frequencies. Hence, the risk of an insufficient number of data points falling within a given wavelength interval is the greatest at the longest wavelengths.

By stacking two or more dispersion images obtained by using the same measurement profile configuration (the same receiver spacing and the same source offset), prior to the dispersion curve extraction, a better defined (i.e. sharper and more continuous) high-amplitude band can in some cases be obtained. Therefore, for computation of a composite curve, it can be advantageous (in order to obtain an increased investigation depth range without having to identify and extract multiple elementary dispersion curves for each source offset) to stack several sets of dispersion images and use the dispersion curves extracted from the stacked images in the subsequent analysis. This can be noticed by inspection of the data presented in Fig. 8. For the $dx = 0.5$ m profile, a maximum combined curve wavelength of 32 m was obtained by using a single stacked dispersion image for each source offset (Fig. 8e), which was the same maximum wavelength as was obtained by using four and six (unstacked) records, respectively, for each source offset (Fig. 8a, b). For comparison, the maximum combined curve wavelength obtained by using one (unstacked) record per source offset (Fig. 8d) was approximately 23 m. Similar observations were made for the other two measurement profile lengths.

5.3. Comparison of combining several dispersion curves and the use of stacking

Fig. 11 shows stacked dispersion images for the Arnarbæli site obtained from data acquired by each of the three measurement profiles, i.e. with $dx = 0.5$ m, $dx = 1.0$ m and $dx = 2.0$ m, respectively, and the two profile combinations ($dx = 0.5$ m/$dx = 2.0$ m and $dx = 0.5$ m/$dx = 1.0$ m/$dx = 2.0$ m). In each case, 16 dispersion images were stacked per receiver spread length (i.e. four records for each receiver spacing/source offset). The stacked dispersion images provide in all cases a relatively well-defined fundamental mode high-amplitude trend; however, a notable break in the high-amplitude band is present in Fig. 11c, and to a slightly lesser extent in Fig. 11d, e.

The dispersion curves that were identified based on the stacked dispersion images in Fig. 11a, c, d (hereafter referred to as "stacked-image-based" curves) are shown in Fig. 12. Furthermore, Fig. 12 provides comparison of the "stacked-image-based" curves and the combined mean dispersion curves obtained on the basis of the same data, either by extracting a single dispersion curve based on each record, or by stacking each set of four dispersion images prior to the dispersion curve identification. Though not shown here, the same characteristics were observed by analysis of the data acquired by the $dx = 1.0$ m profile and by the $dx = 0.5$ m/$dx = 1.0$ m/$dx = 2.0$ m profile combination.

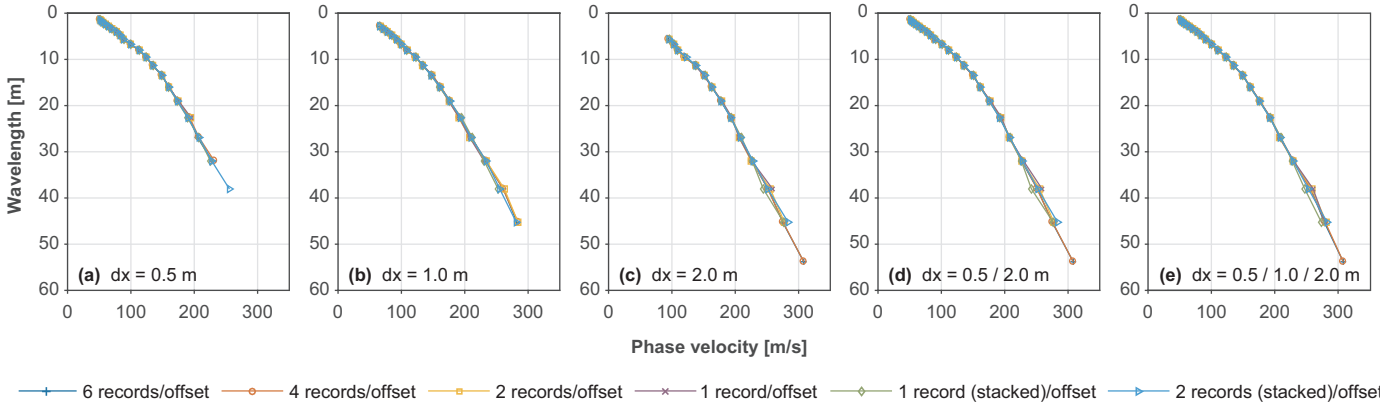

Fig. 10. Combined mean dispersion curves (with $a = 4.0$ in Eq. (6)) obtained for the study cases in Table 2.

Table 2
Overview of studied elementary dispersion curve combinations.

Number of records for each source offset	Profile/combination of profiles				
	dx = 0.5 m	dx = 1.0 m	dx = 2.0 m	dx = 0.5 m/dx = 2.0 m	dx = 0.5 m/dx = 1.0 m/dx = 2.0 m
	Number of elementary dispersion curves				
1[a]	4	4	4	8	12
2[b]	8	8	8	16	24
4[c]	16	16	16	32	48
6	24	24	24	48	72
1 (4 images stacked)[d]	4	4	4	8	12
2 (2 images stacked)[e]	8	8	8	16	24

[a] Record no. 4 for each combination of dx and x_1 (see Table 1 for x_1 values for different dx).
[b] Records no. 4 and 5 for each combination of dx and x_1.
[c] Records no. 2–5 for each combination of dx and x_1.
[d] Dispersion images computed based on records no. 2–5 stacked prior to the dispersion curve identification.
[e] Dispersion images computed based on records no. 2 and 3 and records no. 4 and 5, respectively, stacked prior to the dispersion curve identification.

The results presented in Fig. 12 indicate that similar dispersion curves were obtained by using the three ways of combining/averaging the multichannel surface wave data. However, in some cases (see Fig. 12a, c), the maximum wavelength values of the combined mean dispersion curves were slightly higher than those included in the "stacked-image-based" curves. In general, the low frequency part of the fundamental mode dispersion curve is the most difficult to attain in field measurements carried out using an active seismic source. When multiple dispersion images are stacked (averaged), those containing a less clear low frequency high-amplitude band can cancel out parts of the better defined high-amplitude bands that are present in other images, making the low frequency fundamental mode dispersion trend difficult to identify on the stacked image. Moreover, some breaks were observed in the "stacked-image-based" dispersion curves (see Fig. 12b, c), which correspond to the previously addressed breaks in the high-amplitude bands of the stacked dispersion images (Fig. 11c, d). Hence, the results indicate that, in these cases, a combination of several dispersion curves is more advantageous than the use of a single "stacked-image-based" curve. Furthermore, by averaging the dispersion data after the dispersion curve extraction, it becomes possible to estimate the accuracy of the estimated mean phase velocity values in terms of confidence intervals, as discussed in the following section.

6. Uncertainty associated with the combined mean dispersion curve

The procedure discussed in Section 5 centres on estimating the mean Rayleigh wave phase velocity for each wavelength interval. Point estimates of sample statistics, such as the sample mean, are inevitably subject to error, especially when they are derived based on small sample sizes (here a limited number of elementary dispersion curve data points within a given wavelength interval). Therefore, some variation from the true (population) mean is expected. An interval estimation of the mean phase velocity is a way to supplement the point

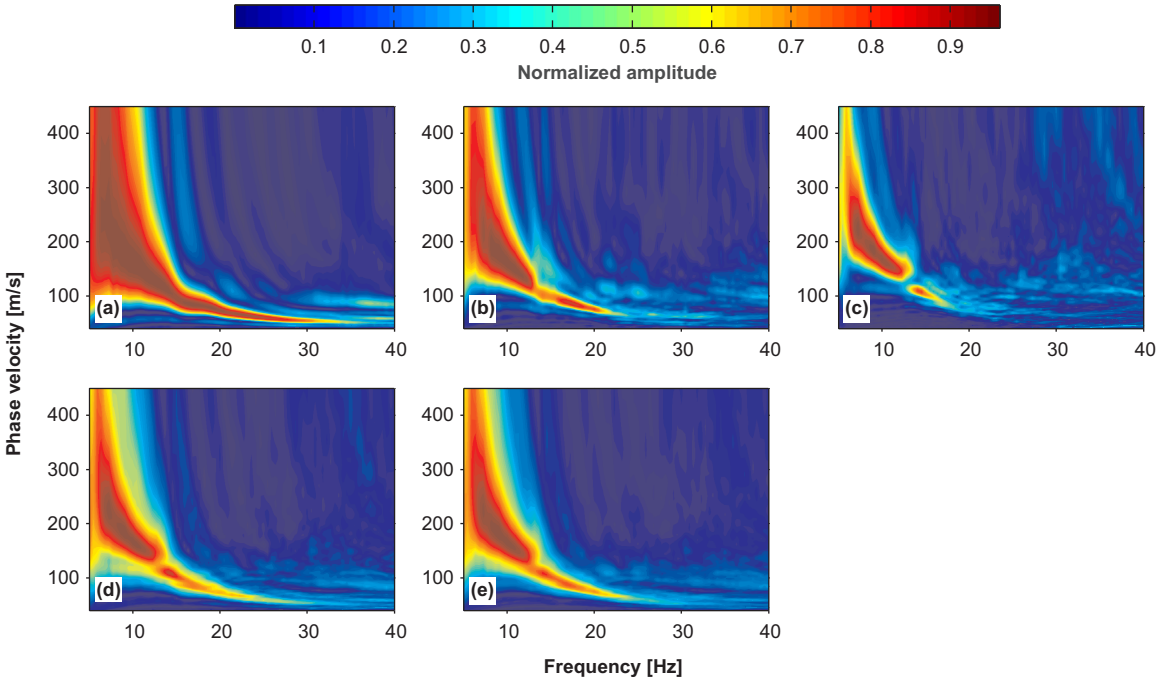

Fig. 11. Dispersion images obtained by stacking (a) 16 dispersion images obtained by the dx = 0.5 m profile (four images for each source offset), (b) 16 dispersion images obtained by the dx = 1.0 m profile (four images for each source offset), (c) 16 dispersion images obtained by the dx = 2.0 m profile (four images for each source offset), (d) 32 dispersion images obtained by the dx = 0.5 m and dx = 2.0 m profiles and (e) 48 dispersion images obtained by the three measurement profiles.

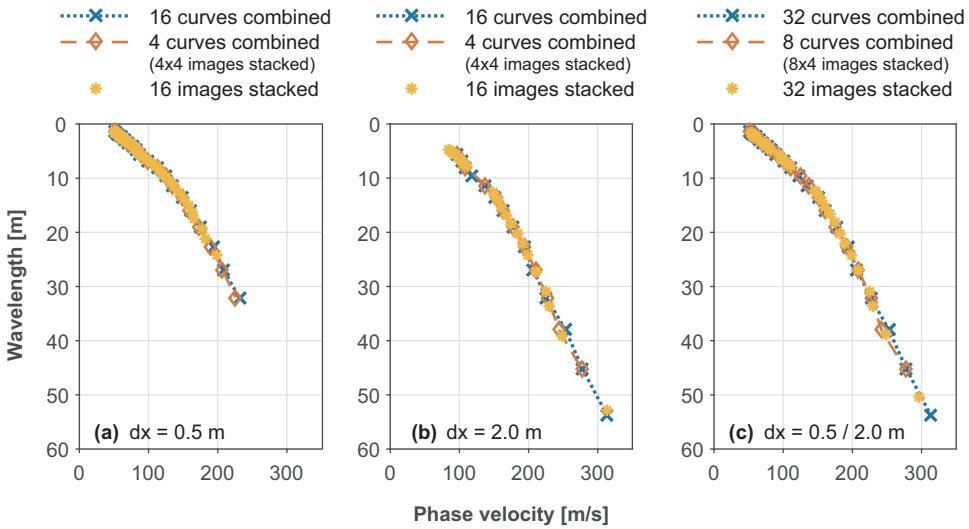

Fig. 12. Comparison of results obtained by combining multiple elementary dispersion curves to form a mean curve (a = 4. 0 in Eq. (6)) and by extracting a single dispersion curve from a stacked dispersion image.

estimate. Using parametric statistical methods, the p% confidence interval (CI) of the mean phase velocity can be obtained by application of the central limit theorem, or based on the t-distribution by assuming a normal distribution of the sample data [50]. The bootstrap is an alternative method for estimation of confidence intervals without distributional assumptions [51,52], and, hence advantageous when the probability distribution of the statistic of interest is unknown or when the sample size is insufficient for application of the central limit theorem (e.g. smaller than 30 data points [50]).

For application of the bootstrap, a Monte Carlo-style sampling is applied on the phase velocity values within each wavelength interval. That is, a large number of resamples, each having the same number of elements as the original sample, is randomly drawn from the original sample with replacement. Hence, the resamples will randomly vary from the original sample. Subsequently, the mean phase velocity value is computed for each resample and the relative frequency distribution of the bootstrap replications used as an approximation of the sampling distribution of the mean phase velocity for the given wavelength interval. Several different types of confidence intervals can be computed based on the simulated replications, e.g. the standard normal bootstrap confidence interval (SB), the percentile bootstrap confidence interval (PB) and the bias-corrected and accelerated (BC_a) confidence interval [52]. SB intervals are computed based on the assumption that the bootstrap replications are approximately normally distributed. The PB interval adjusts for potential bias in the bootstrap distribution, whereas the BC_a method incorporates the effects of both bias and skewness in the confidence interval computations. The three aforementioned methods were used for evaluation of confidence intervals for mean dispersion curves that were obtained by using different elementary dispersion curve combinations. In general, the difference between the three bootstrap confidence intervals (SB, PB and BC_a) was minor and, in many cases, negligible. Hence, in this section, only bootstrap confidence intervals obtained by the BC_a method are presented.

Fig. 13a–c illustrate the distribution of the phase velocity values of the elementary dispersion curve data points acquired by the dx = 0.5 m/dx = 2.0 m profiles at the Arnarbæli station (four records for each receiver spacing/source offset) within three selected wavelength intervals; (a) $\lambda \in$ [8.7,10.4) m, (b) $\lambda \in$ [24.7,29.3) m and (c) $\lambda \in$ [34.9,41.5) m. The wavelength intervals were selected so that they contained different numbers of dispersion curve data points, i.e. 36, 19 and 8 points, respectively. The solid line indicates the point estimate of the mean phase velocity in each case. The dashed lines correspond to plus/minus one standard deviation from the sample mean. However, due to the small sample sizes, it is difficult to draw a conclusion regarding the distribution type of the sample data based on the histograms. Fig. 13d–f show the normal Q-Q plots of the phase velocity

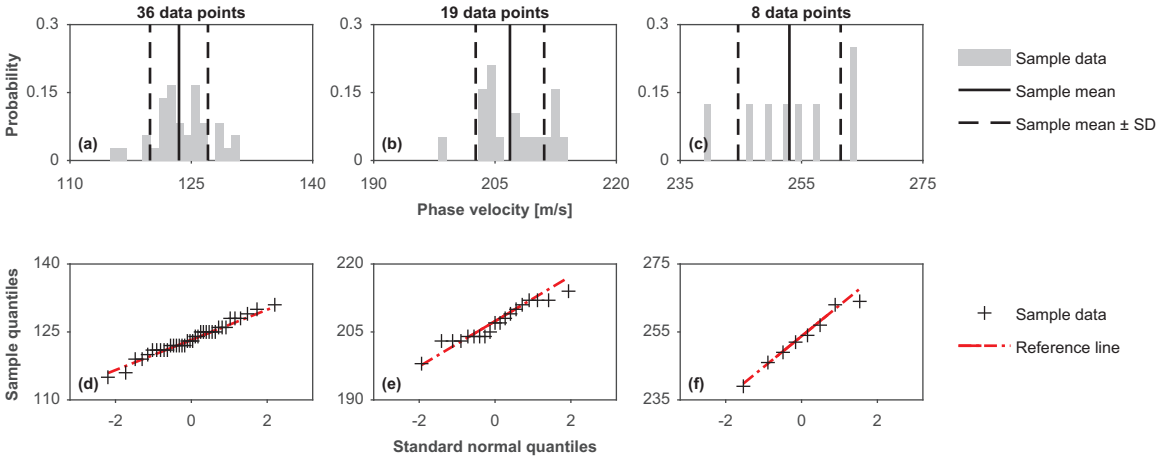

Fig. 13. Probability distributions and normal Q-Q plots of Rayleigh wave phase velocity values within three wavelength intervals (a, d) $\lambda \in$ [8.7, 10.4) m, (b, e) $\lambda \in$ [24.7, 29.3) m and (c, f) $\lambda \in$ [34.9, 41.5) m.

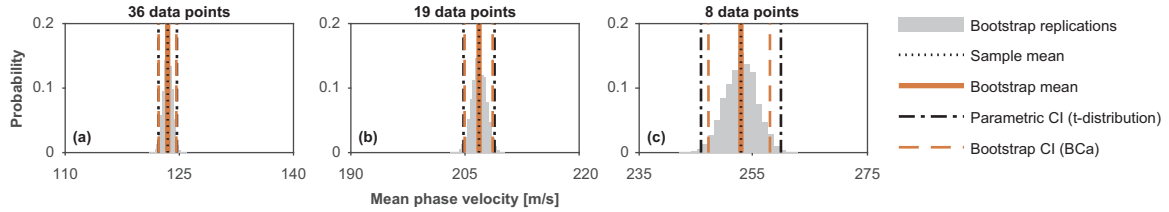

Fig. 14. Bootstrap replications of the sample mean for the wavelength intervals in Fig. 13 along with 95% confidence intervals for the sample mean obtained by using parametric statistics and the bootstrap.

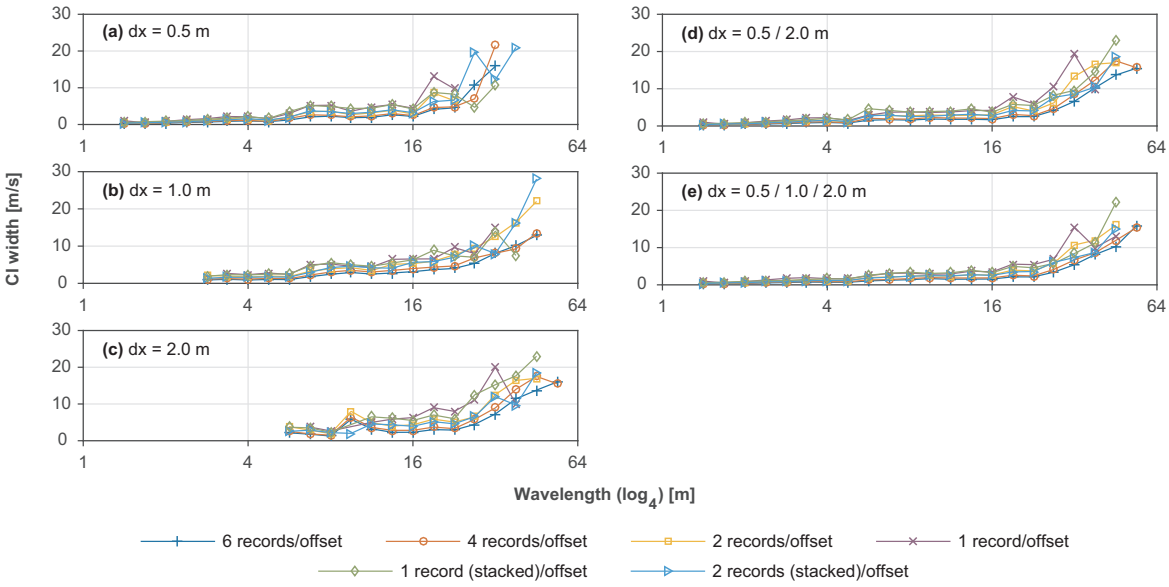

Fig. 15. Width of the 95% BC_a confidence intervals of the combined mean dispersion curves presented in Fig. 10.

values within each of the three wavelength intervals. Overall, the Q-Q plots indicate a fairly linear behaviour of the data, and, hence, that it appears to be justifiable to assume the normal distribution for the phase velocity values in each case. The Shapiro-Wilk test [53] also did not indicate a significant departure from normality at a 5% significance level.

The accuracy of the point estimate of each wavelength interval's mean phase velocity value was evaluated in terms of the 95% confidence interval for the sample mean. Fig. 14 shows the 10,000 bootstrap replications of the sample mean that were obtained for each of the three wavelength intervals in Fig. 13. The bootstrapped mean phase velocity value is shown to match the sample mean for all three intervals. A good match between the bootstrapped and sample mean values was also observed for the other wavelength intervals/elementary dispersion curve combinations that were studied. The dashed lines in Fig. 14 indicate the width of the 95% BC_a confidence intervals for the sample mean. For comparison with the results obtained by the bootstrapping analysis, 95% confidence intervals for the sample mean were also obtained by using the t-distribution. The parametric confidence intervals were, in general, in very good agreement with the bootstrap confidence intervals, even in cases where the number of data points was as little as 10–12. In cases where the number of data points was considerably lower, the parametric confidence intervals were, in general, wider than those obtained by the bootstrap (Fig. 14c). The parametric confidence intervals should, however, be interpreted with caution in cases where the sample size is small and graphical and/or statistical tests carried out for evaluation of the near-normality assumption prior to computations.

Fig. 15 compares the widths of the 95% BC_a confidence intervals for the mean dispersion curves obtained for the study cases reported in Table 2 (Fig. 10). In general, the confidence interval width decreased with decreased wavelength and increased number of observations (i.e. available dispersion curve data points). Hence, by increasing the number of elementary dispersion curves used for computation of the combined mean curve, the width of the confidence intervals generally decreases. However, the observed difference between using four and six records (for each receiver spacing/source offset combination) was in most cases minor, even at longer wavelengths. In cases where only a small number of dispersion curve data points fell into a given wavelength interval, "zigzagging" of the confidence interval width was observed in many cases. Stacking multiple dispersion images and using the dispersion curves extracted from the stacked images in the subsequent analysis provided, in general, similar or slightly narrower confidence intervals than were obtained by using the same number of unstacked records.

7. Effects on shear wave velocity profile estimates

For further assessing the effects of combining elementary dispersion data acquired by receiver spreads of different lengths, as well as the effects of the uncertainty associated with the point estimate of the mean phase velocity for each wavelength interval, Fig. 16 illustrates the inversion of the combined dispersion curves for the (i) $dx = 0.5$ m profile, (ii) $dx = 2.0$ m profile and (iii) $dx = 0.5$ m/$dx = 2.0$ m profiles (six records for each receiver spacing/source offset). Based on the ranges of wavelengths covered by the curves, the approximate maximum investigation depth was estimated according to Eq. (1) (with $\gamma = 1/2$) as 16 m for the $dx = 0.5$ m profile, and 27 m for the $dx = 2.0$ m and $dx = 0.5$ m/$dx = 2.0$ m profiles. The minimum investigation depth, as estimated by Eq. (2) (with $\zeta = 1/2$), was 0.7 m for the $dx = 0.5$ m and $dx = 0.5$ m/$dx = 2.0$ m profiles, and 2.9 m for the $dx = 2.0$ m profile.

Inversion problems involving the dispersion of Rayleigh waves in a

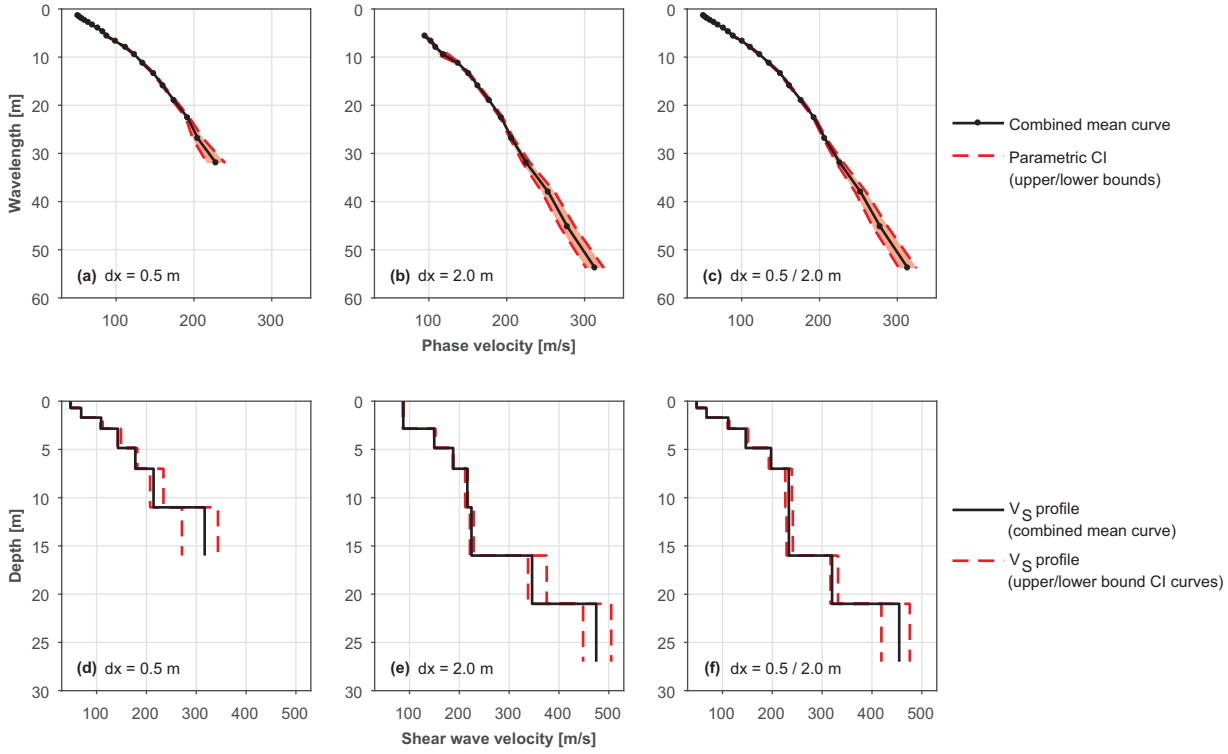

Fig. 16. Combined mean dispersion curves (a = 4. 0 in Eq. (6)) with 95% parametric confidence intervals for the (a) dx = 0.5 m profile, (b) dx = 2.0 m profile and (c) dx = 0.5 m/dx = 2.0 m profiles. Shear wave velocity profiles obtained from the combined mean, upper bound and lower bound dispersion curves, respectively, for the (d) dx = 0.5 m profile, (e) dx = 2.0 m profile and (f) dx = 0.5 m/dx = 2.0 m profiles.

layered elastic medium are by nature both non-linear and non-unique [34]. In short, the inversion is carried out by iteratively comparing theoretical dispersion curves obtained from 'trial' semi-infinite soil layer models to the experimental data (see also Fig. 1). Here, the stiffness matrix method [54] was used for computations of theoretical dispersion curves and a semi-automated trial-and-error procedure [55] used in order to fit the experimental observations with theoretical predictions from assumed soil models. The shear wave velocity of each layer was updated during the inversion process, while the other model parameters were kept unchanged. The misfit (ε) between the theoretical dispersion curve and the experimental curve was evaluated as

$$\epsilon = \frac{1}{Q}\sum_{i=1}^{Q}\frac{\sqrt{(c_{e,i}-c_{t,i})^2}}{c_{e,i}}\cdot 100\% \quad (8)$$

where Q is the number of data points included in the experimental/theoretical dispersion curves, $c_{t,i}$ is the phase velocity value of the i-th data point in the theoretical dispersion curve and $c_{e,i}$ is the phase velocity value of the i-th data point in the experimental curve. A convergence of the search procedure was defined as achieving a misfit of 1.0% or less.

For inversion of each of the three combined mean dispersion curves (Fig. 16a–c), a layered soil model was suggested where the thickness of the top-most soil layer and the depth of the half-space top coincided with the approximate investigation depth ranges obtained with Eqs. (1) and (2). To aid the comparison of the shear wave velocity profiles obtained by using the different experimental curves, the same layering was used in the three inversions, though with a reduced investigation depth for the dx = 0.5 m profile and an increased first-layer thickness for the dx = 2.0 m profile. The initial value of the shear wave velocity for each layer was obtained by mapping the points of the combined mean dispersion curves into approximate values of shear wave velocity [8] and subsequently discretising the resulting pseudo-shear wave velocity profiles to match the previously assumed layer structure. The half-space shear wave velocity was set equal to the shear wave velocity of the bottom-most finite thickness layer throughout the inversion. The compressional wave velocity and the mass density of each layer were estimated based on independent soil investigations [48,49], as well as based on prior knowledge of the Arnarbæli test site. Furthermore, as the Arnarbæli test site is considered normally dispersive, velocity reversals were not permitted during the inversion process.

The resulting shear wave velocity profiles are shown in Fig. 16d–f (solid lines). In general, similar shear wave velocity estimates were obtained by using the three combined mean dispersion curves, though characterized by the different investigation depth ranges. The lack of short wavelength wave components (i.e. λ < 5–6 m) obtained by the dx = 2.0 m measurement profile is reflected by the relatively thick surficial layer in the corresponding shear wave velocity profile (Fig. 16e). At depths greater than 2.9 m, the dx = 2.0 m profile provided very similar shear wave velocity estimates as the dx = 0.5 m/dx = 2.0 m profile. The dx = 0.5 m and dx = 0.5 m/dx = 2.0 m profiles provided nearly the same shear wave velocity values for the uppermost 11 m. However, at depths ranging from 11 m to 16 m, the shear wave velocity estimate obtained with the dx = 0.5 m profile was higher than those obtained by the other profiles.

The shaded areas in Fig. 16a–c illustrate the 95% parametric (t-distribution) confidence intervals for the mean phase velocity within each wavelength interval. The upper and lower bound combined dispersion curves (indicated by the dashed lines in Fig. 16a–c) correspond to the upper/lower bound phase velocity CI values for each wavelength interval. For inversion of the upper and lower bound curves, the shear wave velocity profile obtained from the corresponding mean curve was used as a starting profile for the trial-and-error search procedure. The shear wave velocity profiles obtained by inverting the upper and lower bound combined curves, respectively, are shown using dashed lines in Fig. 16d–f. At wavelengths shorter than 20–25 m, the confidence intervals for the combined mean dispersion curves are very narrow (Fig. 16a–c). Hence, the shear wave velocity estimates obtained from the combined mean curves and the corresponding upper/lower bound

curves were very consistent at shallow depth (Fig. 16d–f). For deeper layers, the wider confidence intervals lead to more differences among the shear wave velocity estimates. This is reflected by the coefficient of variation (Eq. (7)) of the shear wave velocity values for each of the layers, which ranged from 0.1–2.5% for the shallowest layers (i.e. layers at depths less than approximately 5 m) to 5.9–11.8% for the deepest finite-thickness layer included in each profile.

8. Summary and conclusions

This paper presents a methodology for combining dispersion curves that have been extracted from separate MASW dispersion images. The combined experimental dispersion curve is obtained by grouping the elementary dispersion curve data points together within $\log_a$ spaced wavelength intervals. Subsequently, the mean phase velocity within each interval is used as a point estimate of the phase velocity of Rayleigh wave components belonging to the given wavelength range.

Results of MASW field tests conducted at a silty sand test site were used in order to demonstrate the performance and the robustness of the methodology and for evaluation of the number of records and/or different measurement profile configurations needed to obtain a reliable combined mean curve. In the study 24 geophones were used in all cases. The uncertainty of the combined mean curves was evaluated, both by using parametric statistics, assuming the normal distribution for the dispersion curve data points within each wavelength interval, and by the bootstrap. Moreover, the combined dispersion curves were compared to curves extracted from stacked dispersion images. Finally, shear wave velocity profiles obtained by inversion of the combined curves were presented to further assess the effects of the different dispersion curve combinations.

The results of the study indicate that combining multiple dispersion curves that have been gathered by receiver spreads of different lengths at the same site can both increase the maximum depth of the resulting shear wave velocity profile and improve its resolution at shallow depth. Moreover, combination of dispersion data from multiple measurements can help compensate for segments of missing (or limited) data at certain frequencies in individual dispersion images/dispersion curves. Use of a short receiver spread (i.e. $dx = 0.5$ m) and a long receiver spread (i.e. $dx = 2.0$ m) was sufficient for the silty sand site in this study and the intended investigation depth (i.e. 20–30 m). Visual comparison of several dispersion images, acquired by using different measurement profile parameters, can furthermore be essential in order to correctly identify and separate the fundamental mode dispersion curve from overtones or noise, which in some cases may be difficult to do based on a single image. Hence, the use of several source offsets (i.e. three to four) for each receiver spread length can help identification of the fundamental mode trend. For each source offset, around four multichannel surface wave records should be sufficient.

The number of extracted elementary dispersion curves, used for evaluation of the combined mean curve, has to be sufficient to provide a number of, approximately evenly spaced, dispersion curve data points within each wavelength interval. Present experience indicates that the preferred number of data points within each interval is at least five to six, though highly dependent on the interval length and the distribution of the points within the interval. In general, an increased number of dispersion curve data points (within each interval) results in a more precise point estimate of the mean phase velocity. The number and distribution of the elementary dispersion curve data points in the longest wavelength (lowest frequency) range is the main factor affecting the optimum number of wavelength intervals used for computation of the combined curve. The optimum value of the parameter a, which defines the wavelength intervals, should be chosen after initial inspection of the available data. Present experience with applying the methodology indicates that $\log_{5/2}$ to $\log_5$ spaced wavelength intervals are appropriate for most test sites (i.e. $a = 2.5$ to $a = 5.0$ in Eq. (6)). The $\log_3$ or $\log_4$ spaced wavelength intervals (i.e. $a = 3.0$ or $a = 4.0$) will be sufficient in many cases.

Identification and extraction of dispersion curves can be a time-consuming and labour-intensive part of the MASW data processing. As the number of dispersion curve data points, in general, decreases with increasing wavelength, it can be of value to use a higher number of elementary dispersion curves acquired by a longer measurement profile (which should provide the longer wavelength wave components) than by a shorter profile. Moreover, the number of dispersion curves that have to be extracted can be somewhat reduced by stacking several dispersion images, obtained by using the same (or very similar) measurement profile configuration, prior to the (elementary) dispersion curve extraction and the computation of the combined curve. The stacked images can allow more confident dispersion curve extraction and, in some cases, identification of the fundamental mode at higher and/or lower frequencies than can be extracted from a single (unstacked) image. However, in other cases, the dispersion image stacking might not be beneficial as parts of the high-amplitude bands can be cancelled out.

By averaging the dispersion data post dispersion curve extraction, the uncertainty of the combined mean curve estimate can be evaluated and presented by a series of confidence intervals. This enables the analyst to more rationally evaluate the quality of the dispersion data and the combined mean dispersion curve. Furthermore, by inverting the boundary dispersion curves resulting from the confidence interval computations (and/or other combinations of the upper/lower bound phase velocity CI values), the effects of the uncertainty associated with the computation of the mean phase velocity values on the shear wave velocity profile can be studied.

The confidence intervals for the mean phase velocity can, in most cases, be estimated based on the standard error of the elementary dispersion curve data points (within each wavelength interval) by assuming the normal distribution for the sample data. The bootstrap is a useful method for computation of confidence intervals for those wavelength intervals that contain a small number of data points, or in cases where the normal assumption might not be valid. Comparison of series of confidence intervals obtained for different combined mean dispersion curves revealed that the parametric confidence intervals for the mean phase velocity were, in general, in good agreement with the bootstrap confidence intervals. In cases where the number of data points was considerably lower than 10–12, the parametric confidence intervals were, however, somewhat wider than those obtained by the bootstrap.

Although the conclusions presented in this paper are only supported by data from a single test site, the same trend and results can be found in data gathered at a number of other sites. However, relatively similar sand materials characterize the majority of these test sites. Therefore, further measurements will be required in order to conclude about sites characterized by other kinds of soil materials, e.g. fine-grained and/or organic soils.

Acknowledgements

This work was supported by the University of Iceland Research Fund [Grant no. 73077]; the Icelandic Road and Coastal Administration [Grant no. 1800-373]; and the Energy Research Fund of the National Power Company of Iceland [Grant no. NYR-18-2017].

References

[1] Kramer SL. Geotechnical earthquake engineering. Upper Saddle River, NJ: Prentice-Hall; 1996.
[2] CEN. EN1998-1:2004. Eurocode 8: design of structures for earthquake resistance. Part 1: general rules, seismic actions and rules for buildings. Brussels: European Committee for Standardization; 2004.
[3] BSSC. NEHRP (National Earthquake Hazards Reduction Program) recommended seismic provisions for new buildings and other structures (FEMA P-1050-1) 2015 edition. Vol. 1. Part 1: provisions. Part 2: commentary. Washington DC: Federal Emergency Management Agency; 2015.
[4] Gazetas G. Foundation vibrations. In: Fang H-Y, editor. Foundation engineering

handbook. New York, NY: Van Nostrand Reinhold; 1991. p. 553–93.
[5] Aki K, Richards PG. Quantitative seismology: theory and methods 1. San Francisco, CA: W.H. Freeman and Co.; 1980.
[6] Socco LV, Foti S, Boiero D. Surface-wave analysis for building near-surface velocity models – established approaches and new perspectives. Geophysics 2010;75(5):75A83–102A83. http://dx.doi.org/10.1190/1.3479491.
[7] Gabriels P, Snieder R, Nolet G. In situ measurements of shear-wave velocity in sediments with higher-mode Rayleigh waves. Geophys Prospect 1987;35(2):187–96. http://dx.doi.org/10.1111/j.1365-2478.1987.tb00812.x.
[8] Park CB, Miller RD, Xia J. Multichannel analysis of surface waves. Geophysics 1999;64(3):800–8. http://dx.doi.org/10.1190/1.1444590.
[9] Xia J. Estimation of near-surface shear-wave velocities and quality factors using multichannel analysis of surface-wave methods. J Appl Geophys 2014;103:140–51. http://dx.doi.org/10.1016/j.jappgeo.2014.01.016.
[10] Nazarian S, Stokoe II KH, Hudson WR. Use of spectral analysis of surface waves method for determination of moduli and thicknesses of pavement systems. Transp Res Rec 1983;930:38–45.
[11] Xia J, Miller RD, Park CB, Tian G. Inversion of high frequency surface waves with fundamental and higher modes. J Appl Geophys 2003;52(1):45–57. http://dx.doi.org/10.1016/S0926-9851(02)00239-2.
[12] Gao L, Xia J, Pan Y, Xu Y. Reason and condition for mode kissing in MASW method. Pure Appl Geophys 2016;173(5):1627–38. http://dx.doi.org/10.1007/s00024-015-1208-5.
[13] Zhang SX, Chan LS. Possible effects of misidentified mode number on Rayleigh wave inversion. J Appl Geophys 2003;53(1):17–29. http://dx.doi.org/10.1016/S0926-9851(03)00014-4.
[14] Garofalo F, Foti S, Hollender F, Bard PY, Cornou C, Cox BR, et al. InterPACIFIC project: comparison of invasive and non-invasive methods for seismic site characterization. Part I: intra-comparison of surface wave methods. Soil Dyn Earthq Eng 2016;82:222–40. http://dx.doi.org/10.1016/j.soildyn.2015.12.010.
[15] Dikmen Ü, Arısoy MÖ, Akkaya İ. Offset and linear spread geometry in the MASW method. J Geophys Eng 2010;7(2):211–22. http://dx.doi.org/10.1088/1742-2132/7/2/S07.
[16] Ivanov J, Miller RD, Tsoflias G. Some practical aspects of MASW analysis and processing. In: Proceedings of the symposium on the application of geophysics to engineering and environmental problems 2008. Philadelphia, PA; 2008, p. 1186–98. ⟨http://dx.doi.org/10.4133/1.2963228⟩.
[17] Olafsdottir EA, Erlingsson S, Bessason B. Effects of measurement profile configuration on estimation of stiffness profiles of loose post glacial sites using MASW. In: Proceedings of the 17th Nordic geotechnical meeting. Reykjavik, Iceland; 2016, p. 327–36.
[18] Park CB, Miller RD, Xia J. Offset and resolution of dispersion curve in multichannel analysis of surface waves (MASW). In: Proceedings of the symposium on the application of geophysics to engineering and environmental problems 2001. Denver, CO; 2001, p. SSM4. ⟨http://dx.doi.org/10.4133/1.2922953⟩.
[19] Park CB, Miller RD, Miura H. Optimum field parameters of an MASW survey [Exp. Abs.]. In: Proceedings of the 6th SEG-J international symposium. Tokyo, Japan; 2002.
[20] Park CB, Carnevale M. Optimum MASW survey–revisit after a decade of use. In: Proceedings of GeoFlorida 2010: advances in analysis, modeling & design. West Palm Beach, FL; 2010, p. 1303–12. ⟨http://dx.doi.org/10.1061/41095(365)130⟩.
[21] Wood CM, Cox BR. A comparison of MASW dispersion uncertainty and bias for impact and harmonic sources. In: Proceedings of GeoCongress 2012. Oakland, CA; 2012, p. 2756–65. ⟨http://dx.doi.org/10.1061/9780784412121.282⟩.
[22] Xu Y, Xia J, Miller RD. Quantitative estimation of minimum offset for multichannel surface-wave survey with actively exciting source. J Appl Geophys 2006;59(2):117–25. http://dx.doi.org/10.1016/j.jappgeo.2005.08.002.
[23] Zhang SX, Chan LS, Xia J. The selection of field acquisition parameters for dispersion images from multichannel surface wave data. Pure Appl Geophys 2004;161(1):185–201. http://dx.doi.org/10.1007/s00024-003-2428-7.
[24] Yaede JR, McBride JH, Nelson ST, Park CB, Flores JA, Turnbull SJ, et al. A geophysical strategy for measuring the thickness of the critical zone developed over basalt lavas. Geosphere 2015;11(2):514–32. http://dx.doi.org/10.1130/GES01142.1.
[25] Shakir AM, Foti S, Garofalo F, Hijab BR, Laftah AA. Laterally constrained inversion of surface wave data at Najaf city (Iraq). Soil Dyn Earthq Eng 2013;45:89–95. http://dx.doi.org/10.1016/j.soildyn.2012.11.003.
[26] Neducza B. Stacking of surface waves. Geophysics 2007;72(2):V51–8. http://dx.doi.org/10.1190/1.2431635.
[27] Socco LV, Boiero D, Foti S, Wisén R. Laterally constrained inversion of ground roll from seismic reflection records. Geophysics 2009;74(6):G35–45. http://dx.doi.org/10.1190/1.3223636.
[28] Piatti C, Foti S, Socco LV, Boiero D. Building 3D shear-wave velocity models using surface waves testing: the Tarcento basin case history. Bull Seismol Soc Am 2013;103(2A):1038–47. http://dx.doi.org/10.1785/0120120089.
[29] Song X, Gu H. Utilization of multimode surface wave dispersion for characterizing roadbed structure. J Appl Geophys 2007;63(2):59–67. http://dx.doi.org/10.1016/j.jappgeo.2007.04.001.
[30] Lai CG, Foti S, Rix GJ. Propagation of data uncertainty in surface wave inversion. J Environ Eng Geophys 2005;10(2):219–28. http://dx.doi.org/10.2113/JEEG10.2.219.
[31] Cox BR, Bachhuber J, Rathje E, Wood CM, Dulberg R, Kottke A, et al. Shear wave velocity- and geology-based seismic microzonation of Port-au-Prince, Haiti. Earthq Spectra 2011;27(S1):S67–92. http://dx.doi.org/10.1193/1.3630226.
[32] Cardarelli E, Cercato M, De Donno G. Characterization of an earth-filled dam through the combined use of electrical resistivity tomography, P- and SH-wave seismic tomography and surface wave data. J Appl Geophys 2014;106:87–95. http://dx.doi.org/10.1016/j.jappgeo.2014.04.007.
[33] Luo Y, Xia J, Liu J, Xu Y, Liu Q. Research on the middle-of-receiver-spread assumption of the MASW method. Soil Dyn Earthq Eng 2009;29(1):71–9. http://dx.doi.org/10.1016/j.soildyn.2008.01.009.
[34] Foti S, Lai CG, Rix GJ, Strobbia C. Surface wave methods for near-surface site characterization. Boca Raton, FL: CRC Press, Taylor & Francis Group; 2015.
[35] Richart FE, Hall JR, Woods RD. Vibrations of soils and foundations. Englewood Cliffs, NJ: Prentice-Hall; 1970.
[36] Cox BR, Teague DP. Layering ratios: a systematic approach to the inversion of surface wave data in the absence of a priori information. Geophys J Int 2016;207(1):422–38. http://dx.doi.org/10.1093/gji/ggw282.
[37] Pei D. Modeling and inversion of dispersion curves of surface waves in shallow site investigations [Ph.D. Thesis]. Reno, NV: University of Nevada; 2007.
[38] Gucunski N, Woods RD. Use of Rayleigh modes in interpretation of SASW test. In: Proceedings of the 2nd international conference on recent advances in geotechnical earthquake engineering and soil dynamics. St. Louis, MO; 1991, p. 1399–408.
[39] Tokimatsu K, Tamura S, Kojima H. Effects of multiple modes on Rayleigh wave dispersion characteristics. J Geotech Eng 1992;118(10):1529–43. http://dx.doi.org/10.1061/(ASCE)0733-9410(1992)118:10(1529).
[40] Xia J, Miller RD, Xu Y, Luo Y, Chen C, Liu J, et al. High-frequency Rayleigh-wave method. J Earth Sci 2009;20(3):563–79. http://dx.doi.org/10.1007/s12583-009-0047-7.
[41] Yoon S, Rix GJ. Near-field effects on array-based surface wave methods with active sources. J Geotech Geoenviron Eng 2009;135(3):399–406. http://dx.doi.org/10.1061/(ASCE)1090-0241(2009)135:3(399).
[42] Yilmaz Ö. Seismic data processing. Tulsa, OK: Society of Exploration Geophysicists; 1987.
[43] McMechan GA, Yedlin MJ. Analysis of dispersive waves by wave field transformation. Geophysics 1981;46(6):869–74. http://dx.doi.org/10.1190/1.1441225.
[44] Park CB, Miller RD, Xia J. Imaging dispersion curves of surface waves on multichannel record. In: SEG technical program expanded abstracts 1998. New Orleans, LA; 1998, p. 1377–80. ⟨http://dx.doi.org/10.1190/1.1820161⟩.
[45] Dal Moro G, Pipan M, Forte E, Finetti I. Determination of Rayleigh wave dispersion curves for near surface applications in unconsolidated sediments. In: SEG technical program expanded abstracts 2003. Dallas, TX; 2003, p. 1247–50. ⟨http://dx.doi.org/10.1190/1.1817508⟩.
[46] Olafsdottir EA, Erlingsson S, Bessason B. Tool for analysis of multichannel analysis of surface waves (MASW) field data and evaluation of shear wave velocity profiles of soils. Can Geotech J 2018;55(2):217–33. http://dx.doi.org/10.1139/cgj-2016-0302.
[47] Park CB. Imaging dispersion of MASW data – full vs. selective offset scheme. J Environ Eng Geophys 2011;16(1):13–23. http://dx.doi.org/10.2113/JEEG16.1.13.
[48] Green RA, Halldorsson B, Kurtulus A, Steinarsson H, Erlendsson O. A unique liquefaction case study from the 29 May 2008, M_w 6.3 Olfus earthquake, Southwest Iceland. In: Proceedings of the 15th world conference on earthquake engineering. Lisbon, Portugal; 2012.
[49] Olafsdottir EA, Bessason B, Erlingsson S. MASW for assessing liquefaction of loose sites. In: Proceedings of the 16th European conference on soil mechanics and geotechnical engineering. Edinburgh, UK; 2015, p. 2431–6.
[50] Ross SM. Introduction to probability and statistics for engineers and scientists. 4th ed. Burlington, MA: Elsevier Academic Press; 2009.
[51] Efron B. Bootstrap methods: another look at the jackknife. Ann Stat 1979;7(1):1–26. http://dx.doi.org/10.1214/aos/1176344552.
[52] Efron B, Tibshirani RJ. An introduction to the bootstrap. New York, NY: Chapman & Hall; 1993.
[53] Shapiro SS, Wilk MB. An analysis of variance test for normality (complete samples). Biometrika 1965;52(3–4):591–611. http://dx.doi.org/10.2307/2333709.
[54] Kausel E, Roësset JM. Stiffness matrices for layered soils. Bull Seismol Soc Am 1981;71(6):1743–61.
[55] Olafsdottir EA. Multichannel analysis of surface waves for assessing soil stiffness [M.Sc. Thesis]. Reykjavik, Iceland: Faculty of Civil and Environmental Engineering, University of Iceland; 2016⟨http://hdl.handle.net/1946/23646⟩.